Article

Ion Exchange Dialysis for Aluminium Transport through a Face Centered Central Composite Design Approach

Dennis Asante-Sackey [1], Sudesh Rathilal [1], Lingham V. Pillay[2], and Emmanuel K. Tetteh [1,*]

[1] Department of Chemical Engineering, Durban University of Technology, Durban, South Africa
[2] Department of Process Engineering, Stellenbosch University, Matieland, South Africa;
* Correspondence: ektetteh34@gmail.com; Orcid ID: 0000-0003-1400-7847

Abstract: An ion exchange dialysis (IED) is used in the recovery of aluminium from residue. In this papers, the face-centered central composite design (FC-CCD) of the response surface methodology (RSM) and desirability approach is used for experimental design, modelling and process optimization of a counter flow IED system. The feed concentration, feed flowrate, sweep flowrate and sweep concentration are selected as the process variables, with the Al-transport across a Nafion 117 membrane as the target response. A total of 30 experimental runs were conducted with 6 center points. The response obtained was analysed by analysis of variance (ANOVA) and fitted to a second-order polynomial model using multiple regression analysis. The actual R^2 and standard deviation of the model are 0.9548 and 0.2932 respectively. The influences of significant variables are plotted on 3D surface and contour plots. The designed variables were numerically optimized by applying the desirability function to achieve the maximum Al-transport. The optimised condition values were found to be feed concentration (1600 ppm), feed flowrate (61.76%), sweep flowrate (37.50%) and sweep concentration (0.75 N) for the 80% target response at 32hrs. Overall, the model can be used to effectively predict Al-recovery using the designed system.

Keywords: Aluminium; nafion; ion exchange dialysis; response surface methodology (RSM); desirability; enrichment.

1. Introduction

Water is very essential to life and the proper functioning of ecosystems on earth. Due to the global economic drive associated with population growth, water withdrawal pressures from households, industries and agriculture is expected to escalate. The challenge of meeting and efficient distribution across competing water demand from the various sectors can therefore not be an issue of availability, rather availability and quality. The major task of water treatment plants (WTPs) are therefore to meet allowable limits on standards set for water quality parameters.

Coagulation is an important step in urban water treatment schemes that is relatively easy to design, simple to operate and has low energy utilization [1]. The process requires dosing coagulants to coalesce impurities into large masses for subsequent removal by other treatment processes. Common coagulants such as aluminium sulphate, aluminium chloride, poly aluminium chloride, sodium aluminate, ferric chloride and ferric sulphate are used to achieve this physicochemical process in water treatment [2,3]. Aluminium sulphate has been the most widely used coagulant by WTPs. It is known to generate a large amount of water treatment residue. As such, the recovery and utilization of the residue can serve as a secondary source of the coagulant. However, large scale implementation of coagulant recovery by acidification and reuse of the leachate in the 1970's was withdrawn [4]. Similar to alkaline leaching, the process lacks specificity and non-selectiveness. While recovery by pressure driven membrane technique on water treatment residue is faced with fouling issues and high energy demand, the bane of ion exchange resins are fouling by organic compounds and resin regeneration [5,6].

Ion exchange membranes (IEMs) are used in water/wastewater treatment, chemical synthesis and energy harvest and storage [7–9]. These plastic films are classified into cation exchange membranes (CEM) and anion exchange membranes (AEM). The CEMs are embedded with fixed negative charges, and thus permeates ions of opposite charge-counter ions and excludes ions of the same charge- coions. Anion exchange membranes (AEM) have fixed positive charge groups. Their functionality is a combination of membrane permeability and electrochemical properties of ion exchange resins. The CEMs and AEMs are composed of hydrophilic ionic groups and anchored by hydrophobic polymer chains. Notable amongst the hydrophilic functional moieties in CEMs are SO_3^-, PO_3H^-,$-COO^-$, PO_3^{2-}, $C_6H_4O^-$ and NH_3^+, NRH^{2+}, NR_2H^+, NR_3^+ and PR_3^+ for AEMs [10–12].

Ion exchange dialysis (IED), popularly known as Donnan dialysis (DD) employs IEMs for selective transport, removal, and separation of ions of interest. The technology is an electrochemical potentially driven process that separates and concentrates ions from aqueous solutions by the stoichiometric counter transport of ions across the IEM. Ions of interest diffuse from the donor or feed phase to the acceptor or sweep phase. An exchanging electrolyte in the acceptor phase with a higher concentration of the same charge as the ion of interest permeates into the donor phase. The fundamental principle of Fredrick. G Donnan's 1924 study establishesd the donnan equilibrium from the electrostatic repulsion of co-ions from the phases [13]. Electrolytic solutions are at equilibrium when the electrochemical potential difference across the membrane equates to the donnan potential of the membrane [14]. The IED or DD process is not prone to fouling and has a low energy consumption. Another functional primacy of the simple and cost effective IED system is their insignificant electrochemical altering of analyte and enrichment of analyte [15]. These characteristics make it a potentially useful green treatment technology for removal, separation, purification and concentration.

Different commercial IEMs have been used in IED studies including CEMs such as Pall ICE-450 (SA3S and SA3T), Neosepta (CMS, CMX), Selemion (CMV), Ultrex CMI 7000 and Nafion (417 and115) [16–21]. Notable AEMs such as Neosepta (ACS, AMX, AFN and AEX), Ionics (AR204-UZRA and AR103-QPD), Polymerchemie-PC(SA, 100D, acid 60 and acid 100), Fumasep (FTAM and FAB), Jam-1 and Selemion (AMV) have been reported [22–29]. Nafion 117 CEM has been used in the kinetic studies of monovalents such as K^+, Na^+,Cs^+ and divalent Ca^{2+} and Mg^{2+} transport [30–33]. Further records on application of IED using Nafion 117 for Al^{3+} has shown a high recovery of >70% [34]. Despite the high Al-recovery, there is limited information on the effect of process variables on Al-transport through Nafion 117 CEM. A comparative study on the effect of sweep concentration and different membranes (homogeneous Nafion 117 and heterogeneous Ionac 3470) on the recovery was performed using a one-factor at a time (OFAT) approach [35].

As standardization of process variables is quite essential for effective Al-transport, the limitation incorporated with the classical OFAT technique is its incapability in optimizing the overall process in a short time with a lower number of experimental runs for a multivariate system. These inadequacies can be eliminated via a computed statistical standardization viz. Response surface methodology (RSM). The Response surface methodology is a systematic methodology that consists of a group of mathematical and statistical techniques for experimental design, independent and interdependent analysis, model development and exploitation [36,37]. The empirical model (Equation (1)) is a relationship between process variables and the expected response to understand the process mechanism and to optimize the process using minimal experimental runs [38]. Important areas of RSM application are product design, development and formulation and improvement of existing products [39].

$$y = \beta_o + \sum_{n=1}^{n} \beta_i x_i + \sum_{i=1}^{n} \beta_{ii} X_i^2 + \sum_{i}^{i<j,k} \sum_{j,k} \beta_{ijk} x_i x_j x_k + \varepsilon \qquad (1)$$

where y is the transmittance function; β_o is a constant coefficient; β_i, is a linear coefficient β_{ii},is the quadratic coefficient, β_{ijk} is the interaction coefficient, ε is the random error and k is the number of variables studied.

Most commonly used RSM for 3 to a maximum of 6 factors is the central composite design (CCD). This design was originally developed by Box-Wilson. The CCD uses an incomplete full

factorial or fractional factorial to develop the second order polynomial model. For efficient evaluation of first and second order terms and the estimation of curvatures, the CCD arguments the full or factorial design with axial points and replication of center point. The axial points are symmetrical with the center points on the coordinate system at a distance 'α', from the design center. The CCD is made up of the face centered (FC), central composite circumscribed (CCC) and central composite inscribed (CCI). The CCC has axial points that are the same distance 'α', from the center points and the 'α' are used to establish the extremes for low and high limits of each variable. On the other hand, CCI is a scaled down CCF that the limits for each variable as the main limits, uses the limits as the axial points and creates a factorial or fractional factorial design within the limits. However, in the FC, the 'α' is ± 1 such that the axial points are at the center of each face of the factorial space [40,41].

With an industrial concept for aluminium recovery in mind, authors have designed a counter flow IED system for this study. In this present work, the multivariable interactive effect of feed concentration, feed flowrate, sweep concentration and sweep flowrate on Al-permeation using the face centred CCD (FC-CCD) approach is reported. Authors option of the FC-CCD was to operate the process in the extreme region at the corners of the square at three levels for each variable settings. Hence, investigation of the aforementioned parameters within the RSM context allows the evaluation of statistical significance of the variables by a mathematical model equation via F-test for analysis of variance (ANOVA). Mobility of Al with respect to two different time intervals are compared statistically. This therefore provides a basis for the prediction of effects for the target Al-transport at different time zones. Most of the papers on DD or IED have not used the RSM approach and this sets a precedence generally in this field and specifically Al-recovery.

2. Materials and Methods

2.1 Materials and Chemicals

$Al_2(SO_4)_3.18H_2O$ (≥ 97%) and HCl (32% w/w) was supplied by Lichro Chemicals, South Africa. Demineralized water [17.5 MΩ/cm, Purite-HP+BOOST 030773] was used. These reagents were used without further purification. The Nafion 117 with an equivalent weight of 1100 g, thickness 177.8 µm, ion exchange capacity of 0.94 meq/g was used for this experiment. This membrane is a long side chain thermoplastic resin made by the copolymerization of hydrophobic tetrafluorothylene and perfluorovinyl ether which is terminated at the end with a sulfonyl fluoride ($S0_2F$). Preceding acid treatment (3%wt HCl, 90°C, 1hr), the CEM was soaked in demineralized water for 15 mins, heated at 60°C in 3wt% H_2O_2, and rinsed with demineralized water. Further treatment steps included pre and post rinsing with demineralized water after another acid conditioning (1% wt HCl, 25 °C, 180 mins) for 15 mins.

2.2 Experimental design and statistical analysis

Design Expert version 11.1.2 software (State-Ease Inc., Minneapolis, USA) was used for the design, evaluation, mathematical modelling and optimization Figure 1. The independent variables used in this study were: feed concentration (Al; X_1), feed flowrate (%; X_2), sweep flowrate (%; X_3) and sweep concentration (HCl; X_4). The Al^{3+} transport (Y_1) was considered as the dependent factor (response). Performance of the counter flow IED system was evaluated by analysing the Al in the feed and sweep chambers.

The four independent variables were converted into a dimensionless form - X_1, X_2, X_3 and X_4. Three different normalized levels of each variable were designated according to the FC-CCD coding as -1, 0, 1 respectively. Conversion of the selected independent variables into dimensionless codified values is to ensure comparison of factors of different natures with different units and to decrease the error in the polynomial fit according to Equation (2) for the statistical analysis.

$$x_i = \frac{X_i - X_0}{\Delta X} \quad i = 1,2,\dots,k \tag{2}$$

where x_i is the dimensionless coded value of the i-th independent variable, X_i is the un-coded value of the i-th independent variable, Xi is the real value of the independent variable, X_0 is the value of X_i at the center point and ΔX is the step change value of the variable i.

The system's behaviour is defined by the empirical second-order polynomial model [42]. Table 1 shows the independent variables and their respective levels for the FC-CCD used in the present study. The design consists of a first order 2^k factorial portion augmented by 2k axial points and accentor runs (cp), where k is the number of variables. Information about the response system and evaluation of the significance of the factors is mostly achieved at the first order design, [40]. According to the FC-CCD matrix, Table (1), a total of 30 (= 2k + 2k + cp) runs comprising of 16 factorial points, 8 axial points and 6 centre points is required. The remaining five are centre point replication to get a good estimation of the experimental error via the sum of squares. Furthermore, the proposed matrix by the software was randomized in order to prevent systematic error.

Table 1. Coded and actual values of variables of the design of experiments for overall Al-transport optimization.

Symbol	Variable	Coded levels of variables		
		-1	0	1
X_1	Feed concentration (ppm)	100	1050	2000
X_2	Feed flowrate (%)	25	55	85
X_3	Sweep flowrate	25	55	85
X_4	Sweep concentration (N)	0.25	0.625	1

2.3 Ion exchange dialysis set-up

The IED process was conducted using a laboratory flat sheet dialytic set-up equipped with the CEM (Figure 1) with a working area of 205 cm^2. The process involved recirculation of the feed and sweep with a pump of maximum flowrate of 2.6 mLs^{-1}. Pump calibration was performed using a randomized complete block design in order to reduce residual error and controlling nuisance factors. The volume ratio of the feed to the sweep was 2:1. The feed and sweep electrolyte solutions were prepared as provided in Table 1 and homogeneity was ensured during the experiment with the aid of magnetic stirrers. Previous work done by the authors expounds on the choice of the ranges for the variables of concern [43]. All experiments were performed in an air-thermostated room between 22-25 ^oC. The data obtained was evaluated in terms of Al-transport (%) from the feed solution as follows:

$$Y\ (transport)(Al) = \frac{[Al]_{feed(o)} - [Al]_{feed(t)}}{[Al]_{feed(o)}} \times 100\% \qquad (3)$$

where $[Al]_{feed(0)}$ and $[Al]_{feed(t)}$ denote, respectively, the aluminium concentrations at the time at the time t = 0 and at an elapsed time, t, in the feed compartment.

Common sources of leaks that could hinder experiment integrity such as tears in tubes, membrane and inner tubing of peristaltic pumps were checked. Peristaltic pump tubing was replaced periodically to check inner wearing that could be due to the concentration of solutions used. A schematic flow of the experiment for Al-transport is shown in Figure 2.

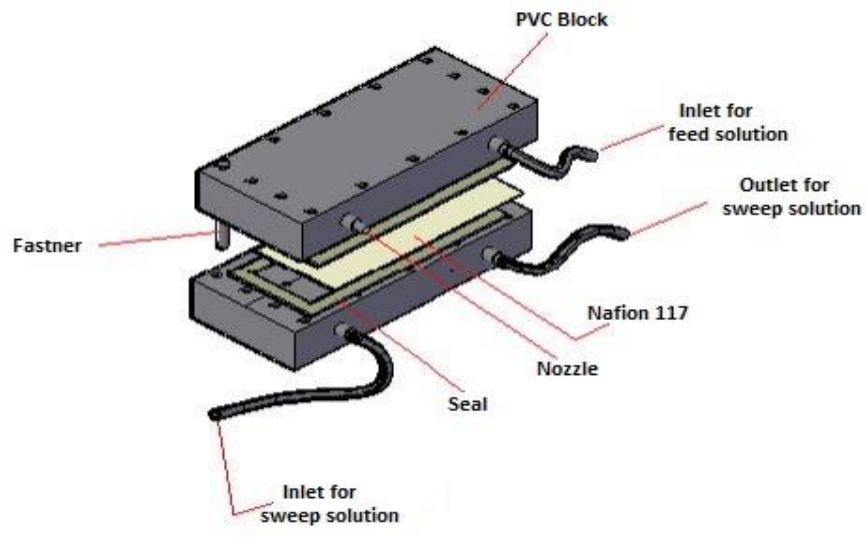

Figure 1. Conceptual design of IED rig.

2.4 Analytical

The Al transport from the feed phase to the sweep phase was measured using the Agilent micro-plasma atomic emission spectrophotometer (MP-AES, MY 18379001). Samples collected from the two phases were diluted (5-100 times) with 1% wt HNO_3 to volume. The total loss of feed and sweep solution due to sampling was between 3% and 4% of the total volume [43].

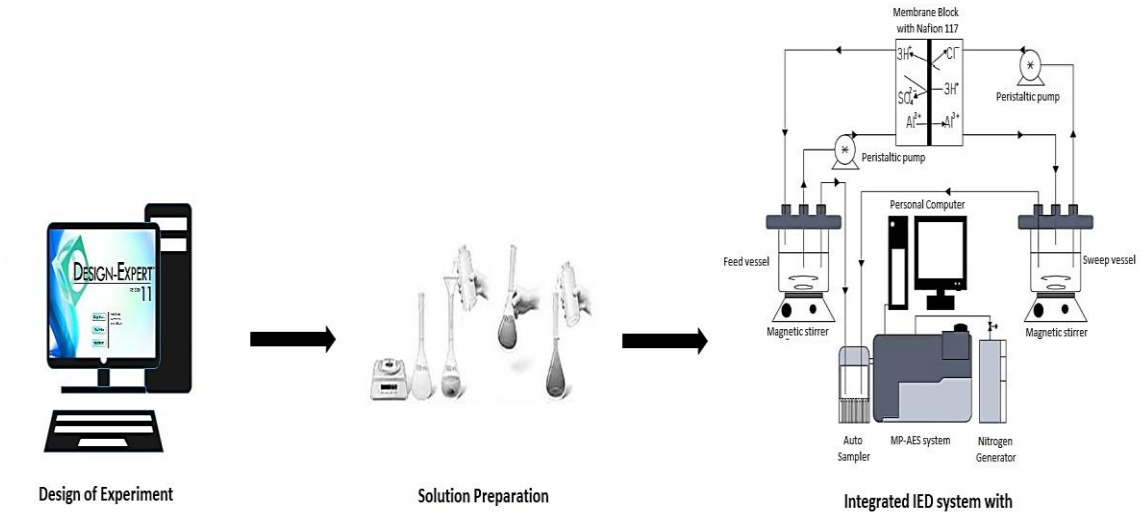

Figure 2. Schematic flow for Al-transport study.

3. Results

The results from the experimental design matrix presented in Table 2 in the randomized order. The Al-recovery at different time intervals showed the effect on each variable at their different interactional levels. Statistical analysis of the response is performed using the various response obtained.

Table 2. Experimental design matrix and observed responses at different time zones.

Run	Variable Level				Response (%)	
Order	X_1	X_2	X_3	X_4	24 hrs	32 hrs
1	1	-1	-1	-1	28.55	35.95
2	1	1	1	-1	33.35	45.65
3	-1	1	-1	-1	75.90	84.10
4	1	-1	1	1	61.6	71.85
5	-1	-1	-1	1	70.2	78.25
6	0	0	0	0	79.1	86.00
7	1	1	-1	1	64.25	73.45
8	-1	-1	1	-1	58.15	61.60
9	-1	1	1	1	86.95	93.55
10	0	0	0	0	78.82	86.05
11	-1	1	-1	1	87.50	94.85
12	0	0	0	0	78.36	85.96
13	0	0	0	0	78.62	85.85
14	1	1	1	1	51.60	63.85
15	-1	1	1	-1	81.40	90.00
16	-1	-1	1	1	57.95	68.75
17	1	1	-1	-1	32.55	32.85
18	1	-1	-1	1	56.95	66.95
19	-1	-1	-1	-1	58.80	65.85
20	1	-1	1	-1	30.25	34.50
21	0	0	0	0	78.98	86.01
22	0	-1	0	0	52.57	60.52
23	-1	0	0	0	78.55	84.98
24	0	0	0	1	84.81	90.19
25	0	1	0	0	72.19	80.71
26	0	0	1	0	66.95	77.33
27	0	0	0	0	78.99	87.12
28	0	0	-1	0	75.90	81.90
29	0	0	0	-1	48.71	54.48
30	1	0	0	0	50.65	58.75

4. Discussion

4.1. Regression models and statistical testing

Statistical analysis of the present Al mobility was performed with analysis of variance (ANOVA). In ANOVA, a comparison was performed for variation due to change in the levels of variables with variations associated to random errors inherent in the measurement of the response (Al-transport). The proportion of influence of a set of variables was therefore assessed towards adequacy and validation of the regression model according to the Fisher test (F-test) and the probability value (p-value at 95% confidence level). As such, the highest order polynomial with significant terms that showed the correlation between variables well and normally (not aliased) would be selected. As shown in Table 3, a high F-value was found with the quadratic vs two factor interaction (2FI) and followed by the linear vs block source. While there was an observed distortion for the cubic vs quadratic model, their F-value and that of 2FI vs linear was insignificant. The model selection was therefore found between quadratic and 2FI. Subsequently, the model selected was based on the low standard deviation (Std. Dev) and the high value of the actual regression coefficient (act-R^2) [44]

Table 3. Sequential model sum of squares for model generation at 32-hrs.

Source	Sum of squares	Df	Mean Square	F value	p-value (prob>F)
Mean vs Total	2130.42	1	2130.42		
Linear vs Block	24.49	4	6.12	12.09	<0.0001

Preprints (www.preprints.org) | NOT PEER-REVIEWED | Posted: 29 November 2019 doi:10.20944/preprints201911.0370.v1

Peer-reviewed version available at Processes 2020, 8, 160; doi:10.3390/pr8020160

2FI vs Linear	4.74	6	0.7899	1.94	0.1316
Quadratic vs 2FI	5.79	4	1.45	16.72	<0.0001
Cubic vs Quadratic	0.7625	8	0.0953	1.32	0.3974
Residual	0.3623	5	0.0725		
Total	2166.56	28			

As shown in Table 4, despite the lower standard deviation and high act-R^2 recorded for cubic model (0.27, 0.99 respectively), the quadratic model showed a better correlation than the cubic, linear and 2FI models. The efficiency of variability in the actual response values can be expounded on by the experimental value and their interactions as given by the act-R^2. However, the acceptable difference between the act-R^2 and the adj.R^2 should be less than 0.2 [39]. Statistically, a high adj.R^2 (>0.75) is acceptable [45].

Table 4. Statistical analysis of the models at 32-hrs.

Response	Source	Standard deviation	Actual R^2	Adjusted R^2	Predicted R^2
Al^{3+} transport	Linear	0.7117	0.6776	0.6216	0.4387
	2FI	0.6376	0.8088	0.6963	0.3961
	Quadratic	0.2941	0.9689	0.9354	0.8034
	Cubic	0.2692	0.9900	0.9459	-3.6866

The selected model in terms of the coded and actual values are provided in Equations (4) and (5) respectively. The coded equation (Equation 4) can be used to make a response prediction for the given coded levels (Table 1) of each process variable. By comparing the coefficients of the terms, the coded equation becomes useful for identifying the relative impact of the terms. The synergetic effect of the model terms are represented by their positive signs (X_2, X_4 and X_1X_4) while the negative signs (X_1, X_1X_2, X_1^2, X_2^2 andX_4^2) indicates the antagonistic effect. The actual values of the model terms in their specified units can be fitted into Equation (5) to predict the Al^{3+} transport at 32-hrs.

Coded equation:

$$\sqrt{Y_{Al}} = +9.20 - 0.8414(X_1) + 0.3718(X_2) + 0.7170(X_4) - 0.2779(X_1X_2) + 0.4334(X_1X_4) - 0.4093(X_1^2) - 0.4693(X_2^2) - 0.4120(X_4^2) \quad (4)$$

In terms of actual values, the model terms are given by;

$$\sqrt{Al}(\%) = 5.26811 - (0.000157 * feedconc.) + (0.079990 * feed\ \ flow) + (4.29677 * Sweep\ \ conc.) - (9.75258E-06 * feed\ \ conc.* feedflow) + (0.001217 * feed\ \ conc.* sweep\ \ conc.) - (4.53502E-07 * feed\ \ conc.^2) - (0.000521 * feed\ \ flow^2) - (2.92973 * sweep\ \ conc.^2) \quad (5)$$

Unlike the synergetic effect of feed concentration in the simplified model developed in the previous work at 24 hrs [43], the feed concentration in the actual model for 32 hrs contributed antagonistically to the Al-recovery. Furthermore, while the quadratic term of sweep concentration was significant at 32 hrs, vice versa was observed at 24 hrs.

4.1.1 Analysis of variance (ANOVA)

The independent variables in the selected model and the impact of each variable were then evaluated. For this purpose, the adequacy of the quadratic model was evaluated using several assessments such as the coefficient of determination, adjusted coefficient and the coefficient of variation (CV). The value of act-R^2 indicates the percentage of the variation in the response that is

attributed to the input variables [46]. In Table 5, the indicated act -R^2 of 0.9548 was close to 1. This represented 95.48% variability of the predicted response value (Al^{3+} transport), which is a function of the four process variables. Also, the adj. R^2 (0.9358) represents 0.0642 of the variations in the response that cannot be attributed to the significant independent terms. The clear exemption of statistically insignificant terms in the model was through the forward screening method under the condition (p-value≤ α = 0.05).

Table 5. ANOVA for reduced quadratic model at 32-hours.

Source	Sum of squares	Df	Mean Squares	F-value	p-value prob>F
Regression model	34.51	8	4.31	50.18	<0.0001
X_1-Feed conc.	12.74	1	12.74	148.28	<0.0001
X_2-Feed flow	2.49	1	2.49	28.95	<0.0001
X_4-Sweep conc.	9.25	1	9.25	107.66	<0.0001
X_1X_2	1.24	1	1.24	14.38	0.0012
X_1X_4	3.01	1	3.01	34.97	<0.0001
X_1^2	0.4585	1	0.4585	5.33	0.0323
X_2^2	0.6027	1	0.6027	7.01	0.0159
X_4^2	0.4645	1	0.4645	5.40	0.0313
Residuals	1.63	19	0.0859		
Pure Error	0.0018	3	0.0006		

Standard deviation = 0.2932; Mean= 8.43; CV %= 3.48;
Actual R^2= 0.9548; Predicted R^2=0.8736 ;Adjusted R^2= 0.9358; Adequate Precision = 22.8386

The ANOVA in Table 5 revealed that the first order (X_1, X_2, X_4), two way interaction (X_1X_2 *and* X_1X_4) and pure quadratic effect (X_1^2, X_2^2 andX_4^2) were highly significant for Al^{3+} transport. More so, the F-value of 50.18 implied the model term was statistically significant and there was only 0.01% chance that the large F-value could be due to noise. F-values of the independent variables X_1, X_2 and X_3 were 148.28, 28.95 and 107.66 respectively. Considering the F-values, the effect of independent variables on Al^{3+} mobility was therefore high for variables with high F-value. The calculated CV of 3.48% further assented to the reliability of the model. A measure of the relative dispersion with respect to the mean provides information on the reproducibility, repeatability and precision of the model, *where*; CV<10% [47,48]. Also, the adequate relationship between the signal–to-noise ratio must exist to inform that the model can be used to navigate the design space. The signal to noise ration given by the adequacy precision, was 22.839 and that was > 4. Therefore the noise level did not compete with useful information from the model.

4.1.2 Diagnostic plots

The predicted versus actual normality probability of residuals and the residuals versus run plot are used to evaluate the goodness-of-fit of the model. The good correlation between the actual and predicted mobility is depicted by the well distribution of the actual values to the predicted value line. The model pred-R^2 and adj. R^2 within 20% was found to be significantly acceptable. Meloun and Militky [49], suggested that a model could be used after a residual analysis has been performed, whereby the residual analysis is used to investigate outliers and detect influential observations. In Figure 3a, the diagnostic plot of the model with the predicted R^2 of 0.8736 showed that data points were close to the diagonal line. Likewise in Figure 3b, the data points of the residuals followed a normal distribution as maximum plots are interlocked with the straight line. Furthering the residual analysis, Figure 3c showed a conformance to a random non-linear scattering trend along the run number and absence of outliers. As such, there was no time related variable lurking at the background. While the negative residual implies an over prediction, a positive residual indicates a low prediction. A plot close to the estimated regression line at zero (0) expounded on the exactness of prediction.

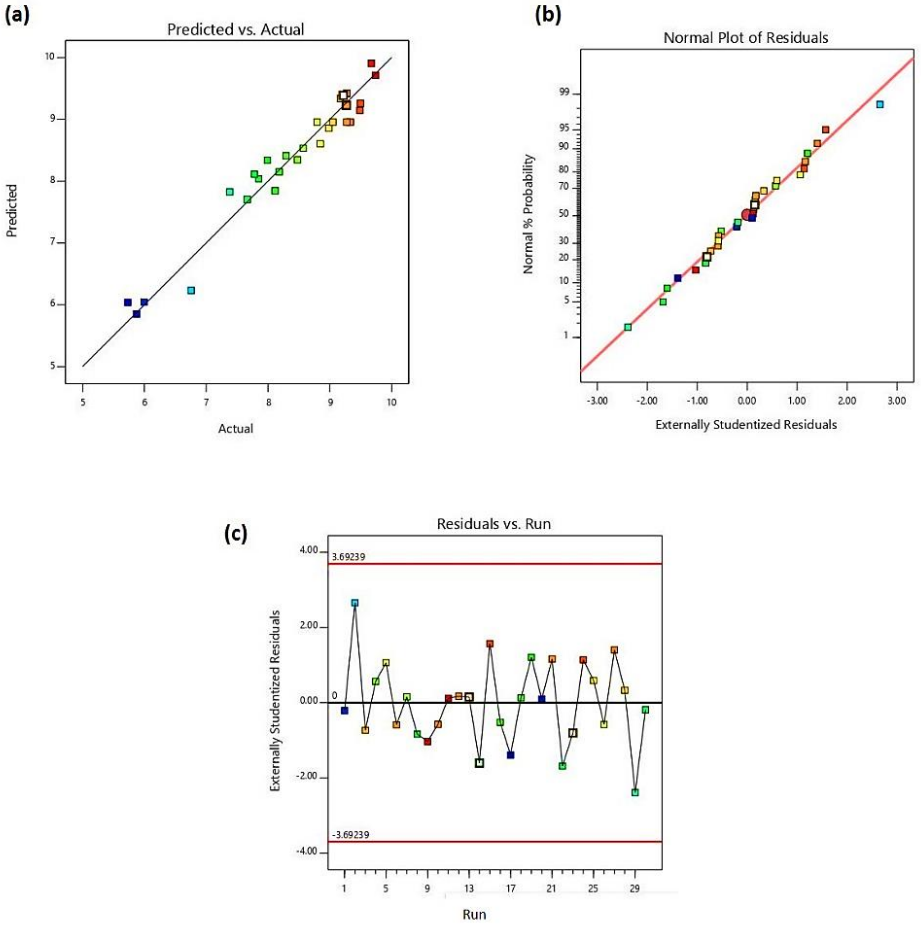

Figure 3. (a) Predicted versus actual values plot; (b) Normal probability plot; (c) Residual versus total run plot.

4.2 Combined effects of operating parameters on the response

Interpretation of the parametric interaction among the process variables was evaluated as combined effects of feed concentration and feed flowrate (X_1X_2); and feed concentration and sweep concentration (X_1X_4). The three dimensional plots (3D-plots) of the regression model were used for the graphical explanation of the interactions. Corresponding response surface plots (RSM) obtained from the Equation (5) are presented in Figures 4(a-c) and 5(a-c). The degree of curvature on the 3D-plots depicts the levels of uncertainties attributed to the parametric interactions. Decision making using the RSM must take into accounts the variable effects on the response and the economic implications. For any good decision, there must be a balance between the considerations. Comparative Al-transport at 24-hrs (Figure 4c and Figure 5c) and 32-hrs was undertaken using contour plot studies.

The concentration polarization effect due to bulk ion distribution at the membrane layer is dominant at high feed concentration. Such an effect reduces selectivity and transmembrane flux [50]. In Figure 4a, increasing flowrate increased Al^{3+} transport at a decreasing feed concentration. At higher flowrates > 55%, the Al-transport ranged between 80 and >90% for a feed range of $100 \leq X_1 \leq 1070$ ppm at 32-hrs study period. An estimated 55-62% transport (Figure 4c) was also observed for decreasing feed concentration from 2000 ppm to about 1740 ppm at 24hrs. As such, a higher feed flowrate does not translate to high mass transport at high feed concentration. Recirculation of feed for a longer time increased the transport as long as the potential difference across the feed and sweep ends existed. A low transport of < 60% was therefore reported between 1930-2000 ppm for a >75% flowrate at 32-hrs (Figure 4b). Under low to mid flow scheme (35-55%), one should expect an

estimated 65- >78.5% Al^{3+} transport from the feed phase with an operating feed concentration of 17450-1340 ppm in 32-hrs.

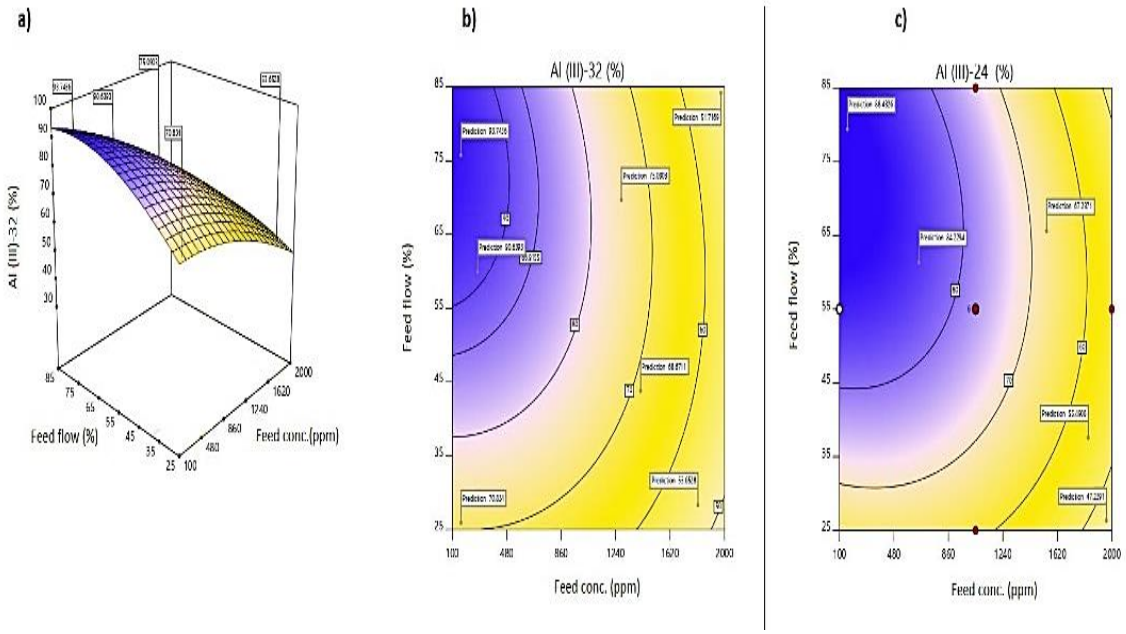

Figure 4. (a) Response surface plot for the interactive effect of feed flow and feed concentration at 32-hrs; (b-c) contour plots of Al-transport as a function of feed flow and feed concentration at 32-hrs and 24hrs respectively.

The potential gradient to draw Al^{3+} increased with increasing sweep concentration. However, the negative impact of the increasing feed concentration was observed again in Figure 5a as the steepest point towards 2000 ppm. The mid to lowest Al-transport occurred at a lower sweep strength for sweep concentration of 0.25-0.38 N HCl. At that sweep concentration range, a transport of 42-54% was observed for feed regions of 1800- >1950 ppm. While attribution of the low Al-transport to the drawing potential of the acid is valid, the bulk distribution at the membrane boundary at high feed concentration could also be a great contributor to the reduced stoichiometric ion exchange. Above 0.48 N HCl, a feed range of 100-1550 ppm resulted in 70- >90% target ion mobility (Figure 5b). Increasing operating concentration above 1N to maximize transport is not advisable. This can result in osmotic dehydration of membrane structure, loss of solute across sweep phase and osmotic transport [51]. The peak point on the curvature of Figure 5a, which reflected as the oval shape in Figure 4b expounds on the high transport (93%-94.1%) being in the region of 0.7-0.81 N HCl for feed concentration ≤ 500 ppm. Observing Figure 5c at 24-hrs, an Al-mobility of 60-68% for a 0.72-0.84 N and 1750-1980 ppm acid and acidic salt solutions respectively. The high points (83-86%) for transport at 24-hrs occurred for a sweep concentration of 0.7-0.84 N and feed concentration of 120- 640 ppm. Therefore, any model generated for 24-hrs would predict within the range of response for Figures 4c and 5c observed (max= 90%). Interactions with sweep flowrate, which singularly has a linear-horizontal effect and others such as X_1X_3 was excluded due to p>0.05.

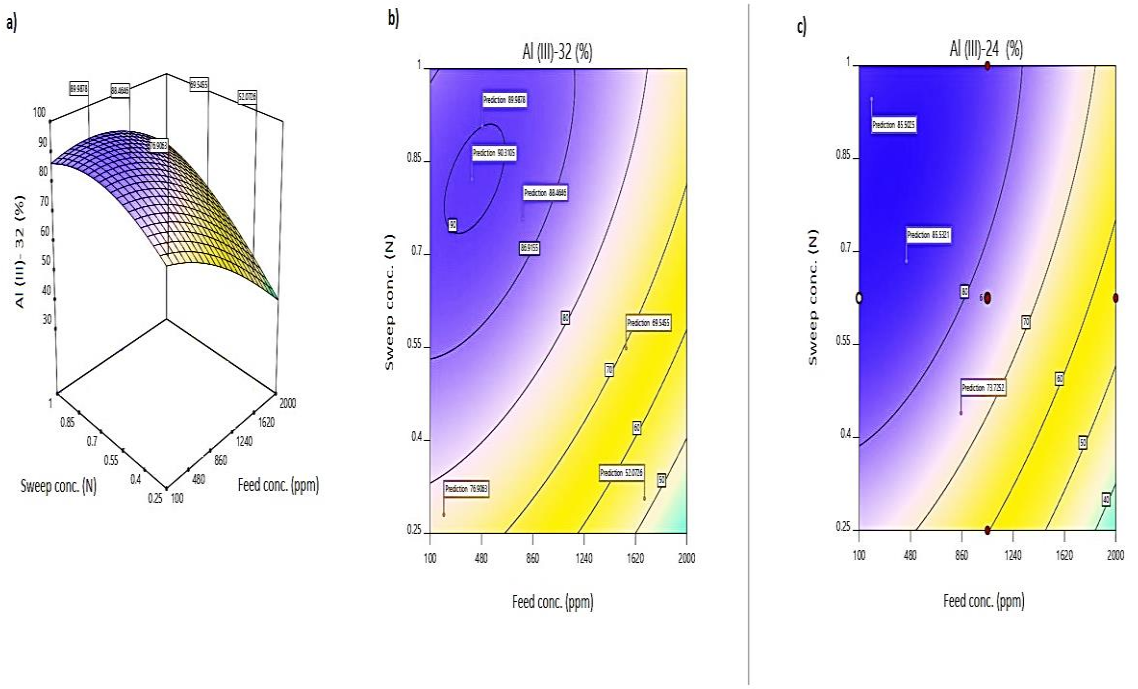

Figure 5. (a) Response surface plot for the interactive effect of sweep concentration and feed concentration at 32-hrs; (b-c) contour plots of Al-transport as a function of feed flow and feed concentration at 32-hrs and 24hrs respectively.

4.3 Enrichment Effect

The enrichment effect of IED and its ability of the process concentrate transporting feed in the final sweep solution sets it apart from other processes. A good idea of the enrichment at the sweep phase is clearly depicted by dividing Al in sweep by initial Al-concentration of the feed. Using 2- 4 N sulfuric acid, and 3:1 feed to sweep volume ratio, 2.4- 3 times enrichment has been reported for Al-recovery from water treatment residue using Nafion 117 [34,35]. Similarly, the enrichment of Al-species at the feed and sweep phase was compared for 24 hrs and 32 hrs respectively for 2:1 feed to sweep phase volume in Figure 6 (a-b). Depending on the other interactions (feed flow and sweep flow), a low feed concentration and low sweep concentration recorded an enrichment factor between 0.95-1.38 and 1.14-1.55 at 24-hrs and 32-hrs respectively. Enrichment for a medium feed and sweep concentration was between 1.24-1.61 for 24-hours and 1.41-1.65 at 32-hrs. Generally, the lower enrichments, < 1.02 was within operating conditions of medium feed- low sweep, high feed- low sweep and high feed-medium sweep concentrations. Furthermore, an observed lowest enrichment factor (0.47), was observed at a high feed and a low sweep concentration. Expectedly, high sweep concentration should translate into high Al-enrichment. However, comparing the enrichment ranges at 24-hrs and 32-hrs for low feed-low sweep concentrations and low feed-high sweep concentrations, dilution of final sweep was evident at the high sweep concentration with enrichments of 1.13-1.39 at 24-hrs and 1.16-1.43 at 32-hrs. A seemingly progressive Al-enrichment with respect to increasing acid (0.25-1 N) ensued at 2000 ppm. Without an overlapping enrichment at each time zone, Al^{3+} highs at 0.25, 0.625 and 1 N were 0.63, 0.90 and 1.19 for 24-hrs and 0.70, 1.01 and 1.33 for 32-hrs respectively.

Preprints (www.preprints.org) | NOT PEER-REVIEWED | Posted: 29 November 2019 doi:10.20944/preprints201911.0370.v1

Peer-reviewed version available at Processes 2020, 8, 160; doi:10.3390/pr8020160

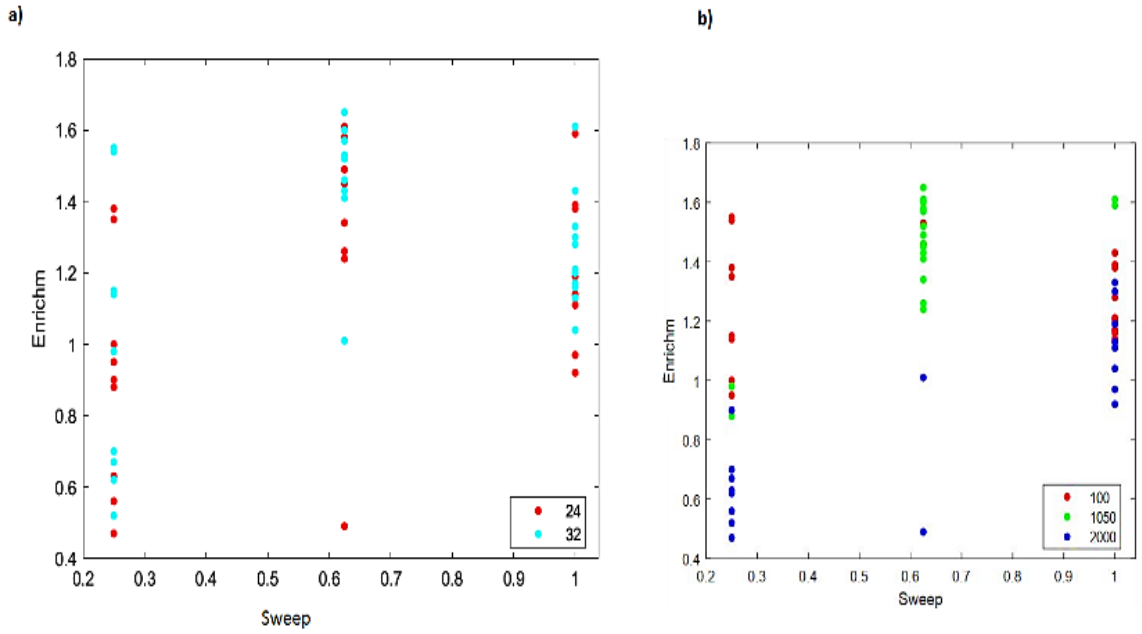

Figure 6. a) Enrichment factor plot for 24 and 32hrs b) Enrichment plot based on feed concentration.

4.4. Desirability

Desirability method is one of the most widely used non-linear programming techniques used to realize multi-objective optimization due to its simplicity and flexibility approach for each response. Responses (y_i) are transmuted into individual scale free desirability with a value range of $0 \leq d_i \leq 1$. A dimensionless desirability value of 0 indicates the response is outside of an acceptable region and the quality of the response is therefore undesirable. Having the response at its goal or target signifies that $d_i = 1$. In Design expert 11.0 worksheet, the goals of the desirability functions of the response are structured into minimum or maximum, within range or target and none. The goals of the factors only are set to exact values. The design variables are then chosen to maximize the overall desirability [52]:

$$D = (d_1 \times d_2 \times \ldots d_n)^{\frac{1}{n}} = (\prod_{i=1}^{n} d_i)^{\frac{1}{n}} \qquad (6)$$

where n is the number of responses in the measure.

The feed concentration, feed flowrate, sweep flowrate and sweep concentration vary in the design range. In this numerical optimization of the counter flow IED system, the input variables were assessed to obtained a desired target Al-transport >75%. Equal importance (3) and weight (1) are assigned for all the process variables and intent. Figure 6 shows the goals (in range for process variables), lower and upper limit (L_l and L_u), optimal value (red dotted for process variables and blue dotted for response) and desirability of the process variables and response. Out of a total of 51 solutions, the optimal parameters to achieve Al-transport for feed concentration, feed flowrate, sweep flowrate and sweep concentration was 1600 ppm, 61.74%, 43.83% and 0.75 N respectively. The optimum results for maximum Al-transport is desirable with a combined desirability of 0.964 which is close to 1. To validate the results and performance of the counter flow IED system, five experimental runs were conducted with optimal values of the process variables. An Al-transport of 77.13% ± 4.19 was observed as compared to the set target of 80% and 78.81% predicted by the model.

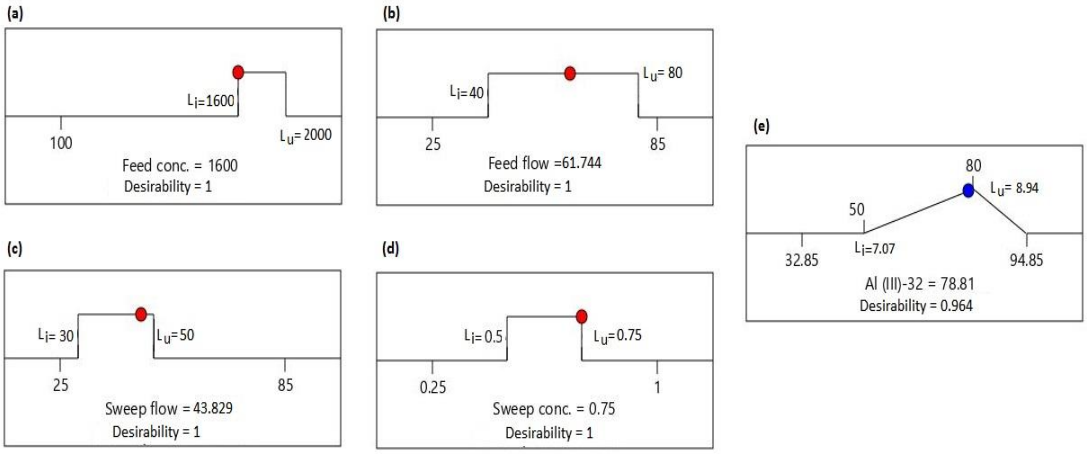

Figure 7. Objective optimization and optimal evaluation for 32hrs Al-transport.

4. Conclusion

The individual and combined effects of four process variables (feed concentration, feed flowrate, sweep flowrate and sweep concentration) on Al- transport in a Nafion 117 membrane was studied using the FC-CCD model of RSM. The desirability approach was developed to carry out Al-transport and optimization. The significant influences of counter flow IED system variables on Al-transport are tested statistically by ANOVA. High adequacy precision ratio (22.839), act. R^2 (0.955) and adj. R^2 (0.936) values indicates the model at 32hrs has a better goodness-of-fit and can navigate through the design space. The regression model for Al-transport is obtained. A strong relation between the experimental and predicted results is shown by the 0.874 pred.R^2 and a standard deviation of 0.29. The interactive influence of the IED variables are illustrated and assessed in 3D surface and contour plots. Increase in feed concentration has a negative effect on Al-transport. Positive impacts are observed with feed flowrate and sweep concentration. The impact of the sweep flowrate is not significant. Enrichment by Nafion 117 on the 2:1 by volume of the counter flow IED system is between 0.47 and 1.65. The optimized parameters of the IED system are obtained to achieve the target transport using the desirability approach. Comparing the validated results to the predicted values by RSM, the optimized IED produces a ± 4.19 and shows that the RSM and desirability approach are reliable. The outcome of this research serves as a baseline to Al-transport study for independent and interacting variables to determine operational periods for optimum recovery at the different times zones of 24 hrs and 32 hrs. Acidification of residue for optimum recovery is reported at different pH and it should be of a future interest to investigate the effect of varied pH and other process variables on Al permeation.

Author Contributions:

Conceptualization, SR and LVP; methodology, LVP and DA-S; software, DA-S and EKT; validation, SR and LVP; formal analysis; DA-S and EKT; investigation, DA-S and EKT; resources, SR and VP, data curation, DA-S; writing-original draft preparation, DA-S and EKT; writing-review and editing, SR; visualization, DA-S; supervision, SR and LVP; project administration, DA-S and EKT; funding acquisition, LVP.

Funding: This research was funded by the Water Research commission-South Africa under the project identification, WRC/240 and the National Research Fund-South Africa, grant number UID-114058.

Conflicts of Interest: Authors declare no conflict of interest

References

1. Bobadilla MC, Lorza RL, García RE, Gómez FS, González EPV. Coagulation: Determination of key operating parameters by multi-response surface methodology using desirability functions. *Water (Switzerland)*. **2019**, 11, 1–21.
2. Barrera-Díaz CE, Balderas-Hernández P, Bilyeu B. Electrocoagulation: Fundamentals and Prospectives. Electrochem. Water Wastewater Treat., *Elsevier*. **2018**, pp. 61–76.
3. Kweinor Tetteh E.; Rathilal S. *Application of Organic Coagulants in Water and Wastewater Treatment*. Org Polym. 2019, 13.
4. Keeley, J.; Jarvis, P.; Judd, S.J. An economic assessment of coagulant recovery from water treatment residuals. *Desalination*. **2012**, 287, 132–137.
5. Nesterenko, P.N. *Ion Exchange-Overview*. 3rd ed. Elsevier Inc.; **2018**.
6. Keeley, J.; Jarvis, P.; Judd, S.J. Coagulant Recovery from Water Treatment Residuals: A Review of Applicable Technologies. *Crit Rev Environ Sci Technol*. 2014, 44, 2675–2719.
7. Pawlowski, S.; Crespo, J.G.; Velizarov, S. Profiled Ion Exchange Membranes: A Comprehensible Review. *Int J Mol Sci*. **2019**, 20.
8. Hassanvand, A.; Wei, K.; Talebi, S.; Chen, G.; Kentish, S. The Role of Ion Exchange Membranes in Membrane Capacitive Deionisation. *Membranes (Basel)*. **2017**, 7, 54.
9. Hagesteijn, K.F.L.; Jiang, S.; Ladewig, B.P. A review of the synthesis and characterization of anion exchange membranes. *J Mater Sci*. **2018**, 53, 11131–11150.
10. Xu, T. Ion exchange membranes: State of their development and perspective. *J Memb Sci*. **2005**, 263, 1–29.
11. Ran, J.; Wu, L.; He, Y.; Yang, Z.; Wang, Y.; Jiang, C. et al. Ion exchange membranes: New developments and applications. *J Memb Sci*. **2017**, 522, 267–291.
12. Luo, T.; Abdu, S.; Wessling, M. Selectivity of ion exchange membranes: A review. *J Memb Sci*. 2018, 555, 429–454.
13. Sarkar, S.; SenGupta, A.K.; Prakash, P. The Donnan Membrane Principle: Opportunities for Sustainable Engineered Processes and Materials. *Environ Sci Technol*. **2010**, 44, 1161–1166.
14. Vanoppen, M.; Stoffels, G.; Demuytere, C.; Bleyaert, W.; Verliefde, A.R.D. Increasing RO efficiency by chemical-free ion-exchange and Donnan dialysis: Principles and practical implications. *Water Res*. **2015**, 80, 59–70.
15. Kim, D.; Judy, J.W. Analysis of Donnan-dialyzer irreproducibility and experimental study of a microfluidic parallel-plate membrane-separation module for total analysis systems. *J Memb Sci*. **2014**, 460:, 148–159.
16. Çengeloğlu, Y.; Kir, E.; Ersöz, M. Recovery and concentration of Al(III), Fe(III), Ti(IV), and Na(I) from red mud. *J Colloid Interface Sci.* **2001**, 244, 342–346.
17. Çengeloğlu, Y.;Kir, E..; Ersoz, M.; Buyukerkek, T.; Gezgin, S. Recovery and concentration of metals from red mud by Donnan dialysis. *Colloids Surfaces A Physicochem Eng Asp*. **2003**, 223, 95–101.
18. Sonoc, A.C.; Jeswiet, J.; Murayama, N.; Shibata, J. A study of the application of Donnan dialysis to the recycling of lithium ion batteries. *Hydrometallurgy*. **2018**, 175, 133–143.
19. Ping Q.; Abu-Reesh, I.M.; He, Z. Boron removal from saline water by a microbial desalination cell integrated with donnan dialysis. *Desalination*. **2015**, 376, 55–61.
20. Okada, T.; Xie, G.; Gorseth, O.; Kjelstrup, S.; Nakamura, N.; Arimura, T. Ion and water transport characteristics of Nafion membranes as electrolytes. *Electrochim Acta*. **1998**, 43, 3741–3747.
21. Miyoshi, H. Diffusion coefficients of ions through ion excange membrane in Donnan dialysis using ions of different valence. *J Memb Sci*. **1998**, 141, 101–110.
22. Pessoa-Lopes, M.; Crespo, J.G..; Velizarov, S. Arsenate removal from sulphate-containing water streams by an ion-exchange membrane process. *Sep Purif Technol*. **2016**, 166, 125–134.
23. Zhao, B.; Zhao, H.; Ni, J. Arsenate removal by Donnan dialysis: Effects of the accompanying components. *Sep Purif Technol*. **2010**, 72, 250–255.
24. Velizarov, S. Transport of arsenate through anion-exchange membranes in Donnan dialysis. *J Memb Sci*. **2013**, 425–426, 243–250.
25. 25. Wiśniewski, J.A.; Kabsch-Korbutowicz, M.; Łakomska, S. Ion-exchange membrane processes for Br − and BrO 3 − ion removal from water and for recovery of salt from waste solution. *Desalination*. **2014**, 342, 175–182.
26. Marzouk, I.; Dammak, L.; Chaabane, L.; Hamrouni, B. Optimization of Chromium (Vi) Removal by Donnan Dialysis. *Am J Anal Chem*. **2013**, 04, 306–313.

27. Turki, T.; Amor, M.B. Nitrate removal from natural water by coupling adsorption and Donnan dialysis. *Water Sci Technol Water Supply*. **2017**, 17, 771–779.
28. Oehmen, A.; Valerio, R.; Llanos, J.; Fradinho, J.; Serra, S.; Reis, M.A.M.; et al. Arsenic removal from drinking water through a hybrid ion exchange membrane – Coagulation process. *Sep Purif Technol* .**2011**, 83, 137–143.
29. Ayyildiz HFF, Kara H. Boron removal by ion exchange membranes. *Desalination*. **2005**, 180, 99–108.
30. Szczepański, P.; Szczepańska, G. Donnan dialysis − A new predictive model for non−steady state transport. *J Memb Sci*. **2017**, 525, 277–289.
31. Agarwal, C.; Chaudhury, S.; Pandey, A.K.; Goswami, A. Kinetic aspects of Donnan dialysis through Nafion-117 membrane. *J Memb Sc*i. **2012**, 415–416, 681–685.
32. Agarwal, C.; Goswami, A. Nernst Planck approach based on non-steady state flux for transport in a Donnan dialysis process. *J Memb Sci*. **2016**, 507, 119-125.
33. Wang, Q.; Lenhart, J.J.; Walker, H.W. Recovery of metal cations from lime softening sludge using Donnan dialysis. *J Memb Sci*. **2010**, 360, 469–475.
34. Prakash, P.; SenGupta, A.K. Selective Coagulant Recovery from Water Treatment Plant Residuals Using Donnan Membrane Process. *Environ Sci Technol*. **2003**, 37, 4468–4474.
35. Prakash, P.; Hoskins, D.; SenGupta, A.K. Application of homogeneous and heterogeneous cation-exchange membranes in coagulant recovery from water treatment plant residuals using Donnan membrane process. *J Memb Sci*. **2004**, 237, 131–144.
36. Adesina, O.A.; Abdulkareem, F.; Yusuff, A.S.; Lala, M.; Okewale, A. Response surface methodology approach to optimization of process parameter for coagulation process of surface water using Moringa oleifera seed. *South African J Chem Eng*. **2019**, 28, 46–51.
37. Tetteh, E.; Amano, K.O.A.; Asante-Sackey, D.; Armah, E. Response Surface Optimisation of Biogas Potential in Co-Digestion of Miscanthus Fuscus and Cow Dung. *Int J Technol.* **2018**, 9, 944.
38. John Babu, D.; King, P.; Prasanna, K.Y. Optimization of Cu (II) biosorption onto sea urchin test using response surface methodology and artificial neural networks. *Int J Environ Sci Technol*. **2019**, 16, 1885–1896.
39. Taran, M.; Aghaie, E. Designing and optimization of separation process of iron impurities from kaolin by oxalic acid in bench-scale stirred-tank reactor. *Appl Clay Sci*. **2015**, 107, 109–116.
40. Kleijnen, J.P.C. Response surface methodology. *Int Ser Oper Res Manag Sci*. **2015**, 216, 81–104.
41. Sahoo, P.; Barman, T.K. ANN modelling of fractal dimension in machining. *Mechatronics Manuf. Eng., Elsevier*, **2012**, 159–226.
42. Iqbal, M.; Iqbal, N.; Bhatti, I.A.; Ahmad, N.; Zahid, M. Response surface methodology application in optimization of cadmium adsorption by shoe waste: A good option of waste mitigation by waste. *Ecol Eng*. **2016**, 88, 265–275.
43. Asante-Sackey, D.; Rathilal, S.; Pillay, L.; Tetteh, E.K. Effect of ion exchange dialysis process variables on aluminium permeation using response surface methodology. *Environ Eng Res* .**2018**. [Accepted].
44. Tetteh, E.K; Rathilal, S. Effects of a polymeric organic coagulant for industrial mineral oil wastewater treatment using response surface methodology (Rsm). *Water SA*. **2018**, 44, 155–161.
45. Owolabi, R.U.; Usman, M.A.; Kehinde, A.J. Modelling and optimization of process variables for the solution polymerization of styrene using response surface methodology. *J King Saud Univ - Eng Sci.* **2018**, 30, 22–30.
46. Siegel, A.F. Multiple Regression. *Pract. Bus. Stat.*, Elsevier; **2012,** 347–416.
47. Nair, A.T.; Ahammed, M.M. The reuse of water treatment sludge as a coagulant for post-treatment of UASB reactor treating urban wastewater. *J Clean Prod*. **2015**, 96, 272–281.
48. Aerts, S.; Haesbroeck, G.; Ruwet, C. Multivariate coefficients of variation: Comparison and influence functions. *J Multivar Anal*. **2015**, 142,183–198.
49. Meloun, M.; Militký, J. Statistical analysis of multivariate data. *Stat. Data Anal*., Elsevier. **2011**, p. 151–403.
50. Luis, P. Introduction. Fundam. Model. Membr. Syst., *Elsevier*. **2018**, 1–23.
51. Davis, T.A. Donnan Dialysis. *Membr. Sep*., vol. 2, Annandale-NJ: Academic Press; **2000**, 1701–1707.
52. Mohapatra, T.; Sahoo, S.S; Padhi, B.N. Analysis, prediction and multi-response optimization of heat transfer characteristics of a three fluid heat exchanger using response surface methodology and desirability function approach. *Appl Therm Eng*. **2019**,151,536–555.